# The reflection-symmetric wiggle of the young protostellar jet HH 211

Chin-Fei Lee<sup>1</sup>, Tatsuhiko I. Hasegawa<sup>1</sup>, Naomi Hirano<sup>1</sup>, Aina Palau<sup>2</sup>, Hsien Shang<sup>1</sup>, Paul T.P. Ho<sup>1,3</sup>, and Qizhou Zhang<sup>3</sup>

#### **ABSTRACT**

HH 211 is a highly collimated jet originating from a nearby young Class 0 protostar. Here is a follow-up study of the jet with our previous observations at unprecedented resolution up to  $\sim 0.3$  in SiO (J = 8 - 7), CO (J = 3 - 2), and SO  $(N_J = 8_9 - 7_8)$ . SiO, CO, and SO can all be a good tracer of the HH 211 jet, tracing the internal shocks in the jet. Although the emissions of these molecules show roughly the same morphology of the jet, there are detailed differences. In particular, the CO emission traces the jet closer to the source than the SiO and SO emissions. In addition, in the better resolved internal shocks, both the CO and SO emission are seen slightly ahead of the SiO emission. The jet is clearly seen on both sides of the source with more than one cycle of wiggle. The wiggle is reflection-symmetric about the source and can be reasonably fitted by an orbiting source jet model. The best-fit parameters suggest that the source itself could be a very low-mass protobinary with a total mass of  $\sim 60~M_{\mathrm{Jup}}$  and a binary separation of  $\sim 4.6$  AU. The abundances of SiO and SO in the gas phase are found to be highly enhanced in the jet as compared to the quiescent molecular clouds, even close to within 300 AU from the source where the dynamical time scale is < 10 yrs. The abundance enhancements of these molecules are closely related to the internal shocks. The detected SiO is either the consequence of the release of Si-bearing material from dust grains or of its formation via gas chemistry in the shocks. The SO, on the other hand, seems to form via gas chemistry in the shocks.

Subject headings: stars: formation — ISM: individual: HH 211 — ISM: jets and outflows.

<sup>&</sup>lt;sup>1</sup>Academia Sinica Institute of Astronomy and Astrophysics, P.O. Box 23-141, Taipei 106, Taiwan; cflee@asiaa.sinica.edu.tw

<sup>&</sup>lt;sup>2</sup> Laboratorio de Astrofísica Estelar y Exoplanetas, Centro de Astrobiología (INTA-CSIC), LAEFF campus, P.O. Box 78, E-28691 Villanueva de la Cañada (Madrid), Spain

<sup>&</sup>lt;sup>3</sup>Harvard-Smithsonian Center for Astrophysics, 60 Garden Street, Cambridge, MA 02138

#### 1. Introduction

Jets from protostars represent one of the most intriguing signposts of star formation. They are believed to be launched from accretion disks around the protostars. They are highly supersonic, collimated, and ballistic. Yet, they are often found to show wiggles in their trajectories. These wiggles of the jets could be due to a precession of the jets (e.g., Raga et al. 1993), or an orbital motion of the jet sources (i.e, the protostars that drive the jets) (e.g., Fendt & Zinnecker 1998; Masciadri & Raga 2002), or both. The jet precession may be due to a precession of the accretion disks because of tidal interactions in noncoplanar binary systems (see, e.g., Terquem et al. 1999) and it can give rise to point-symmetric (i.e., S-shaped) wiggles, while the orbital motion of the jet sources may arise in binaries and it can give rise to reflection-symmetric (i.e., C-shaped) wiggles (Fendt & Zinnecker 1998). Masciadri & Raga (2002) have studied the wiggles of the DG Tau microjet, HH 47, and the Serpens radio continuum jet. Similarly, Anglada et al. (2007) have studied the wiggle of the HH 30 jet. In both cases, assuming that the wiggles of those jets are due to an orbital motion of the jet sources, they have derived orbital parameters and masses that are reasonable for pre-main-sequence binaries. For those jets, however, only one side of the jets is seen, and thus we can not confirm if the wiggles are really reflection-symmetric.

This paper is a follow-up study of the HH 211 jet with our previous observations at unprecedented resolution up to  $\sim 0.3$  (Lee et al. 2009, hereafter Paper I), obtained with the Submillimeter Array<sup>1</sup> (Ho et al. 2004). The jet is clearly seen in SiO (J=8-7) on both sides of a young Class 0 source with more than one cycle of wiggle, and is thus one of the best candidates to study the origin of the wiggle. The wiggle is reflection-symmetric and it seems to be due to an orbital motion of the jet source (Paper I). The wiggle was called the C-shaped bending in Paper I but not here anymore because more than one cycle is seen. In order to have a more complete picture of the wiggle, here we also present CO (J=3-2) and SO ( $N_J=8_9-7_8$ ) emissions of the jet in the same observations as already described in Paper I. By modeling the wiggle, we derive the orbital parameters and then discuss the nature of the source. In addition, we also refine the mass-loss rate of the jet with the CO emission at high resolution and investigate the possible origins of the SiO, SO, and CO emissions in the jet.

<sup>&</sup>lt;sup>1</sup>The Submillimeter Array is a joint project between the Smithsonian Astrophysical Observatory and the Academia Sinica Institute of Astronomy and Astrophysics, and is funded by the Smithsonian Institution and the Academia Sinica.

## 2. Results

In the following, we present the morphology and kinematics of the jet in CO (J=3-2) and SO  $(N_J=8_9-7_8)$  emissions in comparison to those in SiO (J=8-7) emission in Paper I. We also derive the density of the jet from the CO emission and then the abundances of SO and SiO. The systemic velocity in HH 211 is assumed to be  $9.2\pm0.3$  km s<sup>-1</sup> LSR and the distance to the HH 211 is assumed to be  $280\pm40$  pc, as in Paper I. The jet is almost in the plane of the sky with an inclination angle of  $\sim 5^{\circ}\pm3^{\circ}$ . The eastern component of the jet is blueshifted while the western component is redshifted. The eastern component of the jet has a P.A. of  $116.1^{\circ}\pm0.5^{\circ}$ , while the western component has a P.A. of  $297.1^{\circ}\pm0.5^{\circ}$ , indicating that the jet has a small-scale bending,  $\sim 0.5^{\circ}$  to the northeast (Paper I).

# 2.1. Morphology of the jet

Figure 1 shows the CO and SO maps on top of the SiO map of the jet and the 352 GHz continuum map (green contours) of the envelope-disk from Paper I. The CO emission of the jet is derived by excluding the CO emission within  $\sim \pm 10 \ \mathrm{km \ s^{-1}}$  from the systemic, in order to avoid the contamination from the shells and internal shells (for more details, see Lee et al. 2007b). The CO emission of the jet is more than a factor of 4 weaker than the SiO emission. Although the CO emission shows roughly the same morphology as the SiO emission, there are detailed differences (Fig. 1b). The CO emission shows a chain of paired knots on either side of the source SMM1, but with the peaks slightly ahead (i.e., downstream) of the SiO peaks for most of the better resolved knots (see, e.g., knots BK2, BK3, and RK2 in Fig. 1c). The CO emission also shows the same curvy structures for knots BK1 and RK1, and the same reflection-symmetric wiggle of the jet (Figs. 1b, c) as SiO. However, the CO emission extends closer in to the source than the SiO emission, with the closest peaks (labeled as knots RK0 and BK0 in Fig. 1c) at  $\sim 0.4$  ( $\sim 100$  AU) on either side of the source. The SO emission is even weaker than the CO emission, but it also shows knotty structures along the jet, like the CO emission (Fig. 1a). Like the CO peaks, the SO peaks also appear slightly ahead of the SiO peaks in e.g., knots BK2, BK3, and RK2. However, almost no SO emission is seen toward the innermost pair of CO knots.

## 2.2. Kinematics along the jet axis

Figure 2 shows the position-velocity (PV) diagram cut along the jet axis in CO for the two inner pairs of knots, e.g., BK0, BK1, RK0 and RK1, in comparison to that in SiO. The

innermost pair of CO knots, BK0 and RK0, allow us to study the jet kinematics closer to the source than the innermost pair of SiO knots, BK1 and RK1. They are seen associated with a broad range of velocities, tracing the internal shocks closer to the source than the SiO knots. The four sub-knots of BK1 and RK1 seen in SiO with a range of velocities (see Paper I) have possible counterparts in CO in the PV diagram (Fig. 2, marked with yellow lines and question marks). The separation between the first SiO sub-knots and the innermost pair of CO knots is  $\sim 0.99$  (or  $\sim 220$  AU), roughly the same as that in between the sub-knots. This suggests that the innermost pair of CO knots and the sub-knots of BK1 and RK1 are all the internal shocks produced by the same mechanism, namely by a periodical variation in the jet velocity as suggested in Paper I.

The knots BK2 and BK3 are better resolved, allowing us to study the detailed kinematics in different emissions in the internal shocks. Figure 3 shows the PV diagrams cut along the jet axis in CO, SiO, and SO for these knots. In SiO, these knots clearly show a head-tail morphology, with the heads associated with a broad range of velocities and thus tracing the internal shocks. With respect to the mean velocity of the jet reported in Paper I, the nearside of the heads is blueshifted and the farside is redshifted, because of the sideways ejection of the jet material in the shocks (see also Santiago-Garcia et al. 2009). In the heads of these knots, the CO emission appears ahead of the SiO emission and the velocity range of the CO emission is smaller than that of the SiO emission. Since SiO emission traces denser and warmer regions than CO emission, these differences suggest that the SiO emission traces stronger shocks closer to the shock front and the CO emission traces the weaker shocks in the downstream. As for the SO emission, only knot BK3 is bright enough for kinematic study. In that knot, the SO emission is slightly ahead of the SiO emission with a smaller velocity range, tracing weaker shocks than the SiO emission. Also, the SO emission seems slightly behind (i.e., upstream) the CO emission and peaks at higher velocity offsets from the mean jet velocity than the CO emission, tracing stronger shocks than the CO emission.

# 2.3. Column and Volume Densities of the jet

The column and volume densities of the jet can be estimated from the CO emission of the two innermost pairs of knots (i.e., knots BK0, BK1, RK0, and RK1). At the resolution of  $\sim 0.46 \times 0.36$ , the mean intensity of the CO emission toward these knots is  $\sim 3.2$  Jy beam<sup>-1</sup> km s<sup>-1</sup> (see Fig. 1b). The abundance of CO relative to H<sub>2</sub> is assumed to be  $\sim 4 \times 10^{-4}$  as if the CO gas is formed via gas-phase reactions in an initially atomic jet (Glassgold et al. 1991, see also §4.3). The kinetic temperature the CO emission can be assumed to be 200 K, slightly lower than the kinetic temperature derived from the CO

emission in much higher transitions in the far infrared, which was found to be  $\gtrsim 250$  K (Giannini et al. 2001). Assuming LTE, the excitation temperature of the CO emission can be assumed to be the same as the kinetic temperature. Assuming that the CO emission is optically thin, the column density of the jet in H<sub>2</sub> is  $N \sim 5.5 \times 10^{20}$  cm<sup>-2</sup>. However, the true column density of the jet is actually higher because the jet is spatially unresolved perpendicular to the jet axis. With the beam having a size  $b \sim 0''.45$  or 125 AU perpendicular to the jet axis and the jet having a deconvolved width  $\lesssim 40$  AU (derived from the SiO jet in Paper I), the true column density of the jet is  $N_a \gtrsim N(125/40) \sim 1.7 \times 10^{21}$  cm<sup>-2</sup>. As a result, the volume density of the jet is  $n \gtrsim N_a/40$ AU  $\sim 2.8 \times 10^6$  cm<sup>-3</sup>, about two orders of magnitude higher than the critical density of CO (J = 3 - 2) line, which is  $3 \times 10^4$  cm<sup>-3</sup> at 200 K. On the other hand, the volume density derived here is one order of magnitude lower than the critical density of the SO line, and two orders of magnitude lower than that of the SiO line at 200-500 K. Note that the critical densities here are derived using the collisional rate coefficients listed in the Leiden Atomic and Molecular database (Schöier et al. 2005).

# 2.4. SO and SiO abundances in the jet

The abundances of SO and SiO relative to  $H_2$  can be estimated by dividing SO and SiO column densities by that of  $H_2$  derived from the CO emission, respectively. However, since the SO and SiO emissions trace stronger shocks and thus denser material than the CO emission, the abundances estimated here are likely to be the upper limits.

At the resolution of 0".46×0".36, the mean SO intensity toward the innermost pair of SO knots (i.e., knots BK1 and RK1) is  $\sim 1$  Jy beam<sup>-1</sup> km s<sup>-1</sup> (see Fig. 1a). The excitation temperature of the SO emission is assumed to be the same as that of the CO emission, but it could be higher because the SO emission seems to trace stronger shocks than the CO emission as seen in knot BK3 in the downstream (see §2.2). Assuming that the SO emission is optically thin, the SO column density is  $\sim 1.1 \times 10^{15}$  cm<sup>-2</sup>. Therefore, the abundance of SO is  $\sim 2 \times 10^{-6}$ . It is  $\sim 400$  times that in cold quiescent clouds (cores), e.g., TMC-1, which is  $\sim 5 \times 10^{-9}$  (Ohishi & Kaifu 1998).

At the resolution of  $0\rlap.{''}46\times0\rlap.{''}36$ , the SiO intensity toward the innermost pair of SiO knots decreases rapidly with the distance from the source from  $\sim 20$  to 5 Jy beam<sup>-1</sup> km s<sup>-1</sup> (Fig. 1a). Assuming an excitation temperature of 500 K and optically thin emission as in Paper I, the SiO column density at the SiO knots is  $(4.4-1.0)\times10^{15}$  cm<sup>-2</sup>, resulting in a SiO abundance of  $(8-2)\times10^{-6}$ . Therefore, the SiO abundance is highly enhanced by about five orders of magnitude over that in quiescent molecular clouds where the abundance of SiO is  $\lesssim 10^{-11}$  (Ziurys et al. 1989).

# 3. An orbiting source jet model for the wiggle

The reflection-symmetric wiggle of the jet could be due to an orbital motion of the jet source in a binary system (Fendt & Zinnecker 1998; Masciadri & Raga 2002). If that is the case, then by modeling the wiggle of the jet, we could obtain the parameters of the orbital motion and then discuss the nature of the source (see §4.1). To model, we adopt the right-handed Cartesian coordinate system as shown in Figure 4, with the +z-axis aligned with the eastern component of the jet. For simplicity, the jet source is assumed to have a circular orbit in the x-y plane, with the jet propagating ballistically in the z-axis at a velocity of  $v_j$ . The orbit has a period  $P_o$ , an orbital velocity  $v_o$ , and a radius  $R_o$ . Assuming that the orbital motion of the jet source is in the same direction as the rotation motion of the HCO<sup>+</sup> envelope-disk (Paper I), we have  $v_o > 0$  (i.e., positive for right-handed orbital motion). Then for a jet lying close to the plane of the sky as in the case of HH 211, the trajectory of the jet in the plane of the sky can be approximately given by

$$x = -\sqrt{R_o^2 + (v_o \frac{z}{v_j})^2} \cos[\phi_0 - \frac{v_o}{R_o} \frac{z}{v_j} + \tan^{-1}(\frac{v_o}{R_o} \frac{z}{v_j})] + \eta z$$
(1)

where  $\phi_0$  is the current phase angle of the jet source in the orbit measured from the +x-axis toward the +y-axis direction, and  $\eta$  is to account for the small-scale bending of the jet to the northeast (Paper I). Define the periodic length as

$$\Delta z \equiv v_{\rm j} P_{\rm o} \tag{2}$$

and the velocity ratio as

$$\kappa \equiv \frac{v_{\rm o}}{v_{\rm j}},\tag{3}$$

we have

$$R_{\rm o} = \frac{v_{\rm o} P_{\rm o}}{2\pi} = \frac{\kappa \triangle z}{2\pi} \tag{4}$$

and thus

$$x = -\sqrt{\left(\frac{\kappa \Delta z}{2\pi}\right)^2 + (\kappa z)^2} \cos(\phi_0 - \frac{2\pi z}{\Delta z} + \tan^{-1} \frac{2\pi z}{\Delta z}) + \eta z$$
(5)

When  $z \gg \frac{\triangle z}{2\pi}$ , we have

$$x \approx -\kappa z \cos(\phi_0 - \frac{2\pi z}{\Delta z} + \frac{\pi}{2}) + \eta z \tag{6}$$

which means that the wiggle due to the orbital motion of the jet source has an opening angle  $\alpha \approx 2\kappa$ . Figure 5 shows the best fit of this model to the SiO, CO, and SO data simultaneously. As can be seen, the wiggle of the jet can be reasonably fitted by this model. The best-fit parameters are  $\Delta z = 1530 \pm 25$  AU ( $\sim 5''.46 \pm 0''.09$ ),  $\kappa = 0.0094 \pm 0.0007$  (or  $0.54^{\circ}\pm0.04^{\circ}$ ),  $\phi_0 = 155^{\circ}\pm13^{\circ}$ , and  $\eta = 0.0098\pm0.0009$  (or  $0.56^{\circ}\pm0.05^{\circ}$ ). Thus,  $R_o \sim 2.3\pm0.2$  AU,  $v_o \sim 1.60 \pm 0.56$  km s<sup>-1</sup>, and  $P_o \sim 43 \pm 23$  yrs, assuming that  $v_j = 170 \pm 60$  km s<sup>-1</sup> as in Paper I. In this model, the wiggle of the jet has an opening angle of  $\alpha \sim 1.1^{\circ}$ , similar to that seen in the observations (Fig. 5). About 3 cycles of wiggle are seen on each side of the source. The specific angular momentum for the orbital motion is  $\sim 3.7\pm1.3$  AU km s<sup>-1</sup>, comparable to that of the jet rotation yet to be confirmed, which is  $\lesssim 5$  AU km s<sup>-1</sup> (Paper I).

#### 4. Discussion

## 4.1. SMM1: A very low-mass protobinary?

It has been argued that almost all stars must form in binary or multiple systems because of the fragmentation of star-forming dense molecular cores (Goodwin et al. 2007). Could the source SMM1 itself be a protobinary in the Class 0 phase (i.e., the early phase of star formation) since the wiggle is reasonably reproduced by an orbiting source jet model? In order to investigate this possibility, we evaluate here the possible mass of the source, assuming that the source is a binary. Let  $M_j$  be the mass of the jet source,  $M_c$  be the mass of the companion, and m be the mass ratio of the jet source to the companion, i.e.,  $M_j = mM_c$ , then the binary separation is  $a = (1 + m)R_o$ . From the Kepler's 3rd law of orbital motion, the total mass of the binary in terms of the model parameters is then

$$M_t \approx 9.5 \times 10^{-4} (1+m)^3 \times (\frac{v_{\rm j}}{100 \text{ km s}^{-1}})^2 (\frac{\kappa}{1^{\circ}})^3 \frac{\Delta z}{100 \text{ AU}} M_{\odot}$$
 (7)

With the best-fit values of  $\kappa$  and  $\Delta z$ , and the jet velocity  $v_{\rm j} = 170 \ {\rm km \ s^{-1}}$ , we have

$$M_t \approx 6.9 (1+m)^3 M_{\text{Jup}} \tag{8}$$

To determine the value of m, we resort to the previous estimation of the mass of the source. Previously, the mass of the source has been estimated to be  $\sim 60~M_{\rm Jup}$  from an evolutionary model (Froebrich et al. 2003). This mass is also consistent with that derived from the HCO<sup>+</sup> rotating envelope-disk, assuming that the rotation is Keplerian (Paper I). If we adopt this

mass as the total mass of the binary, then  $m \approx 1$ . This value of m is in good agreement with that found in the binaries of very low-mass stars and brown dwarfs (Close et al. 2003; Bouy et al. 2006), which tend to have equal mass companions. In addition, the binary separation would be  $2R_o \sim 4.6$  AU, also consistent with that found in those binaries (Close et al. 2003; Bouy et al. 2006), which have a range of separation between 0-30 AU. Therefore, SMM1 itself could indeed be a very low-mass protobinary because of the fragmentation at the beginning of star formation (see, e.g., Machida et al. 2008b). It is unclear, however, why the jet source, with only  $\sim 30~M_{\rm Jup}$ , can have such an energetic collimated jet, but the companion as massive as the jet source does not have a jet or an outflow. It is also unclear if this protobinary will remain substellar in the final stage since it is surrounded by a compact envelope with an estimated mass of  $\sim 50~M_{\rm Jup}$  (although it is a lower limit, see Lee et al. 2007b) at the eastern edge of the ammonia envelope (Paper I)? Also, since the source SMM1 could form a triple system with the source SMM2 detected at  $\sim 84$  AU to the southwest with a planetary mass (Paper I), could the source SMM2 be ejected from the SMM1 binary system in the early stage of star formation because of dynamical decay (Goodwin et al. 2007)? The HH211, if indeed a triple system consisting of a close binary (<30 AU) with a third component at  $\sim 100 \text{ AU}$ , would be quite similar to those found in Upper Scorpius by Bouy et al. (2006).

#### 4.2. The mass-loss rate and accretion rate

Here we estimate the mass-loss rate of the jet and the accretion rate toward the central source, in order to compare their ratio with that predicted in the current jet launching models. The (two-sided) mass-loss rate of the jet can be given by

$$\dot{M}_i \sim 2v_i m_{\rm H_2} Nb \tag{9}$$

where N and b are the column density of the jet and the beam size perpendicular to the jet axis, respectively, as given in §2.3, and  $m_{\rm H_2}$  is the mass of an H<sub>2</sub> molecule. With the jet velocity  $v_j \sim 170$  km s<sup>-1</sup>, the mass-loss rate is  $\dot{M}_j \sim 1.8 \times 10^{-6}~M_{\odot}~\rm yr^{-1}$ , as found in Lee et al. (2007b). The mechanical luminosity of the jet is then

$$L_j = \frac{1}{2}\dot{M}_j v_j^2 \sim 4.3L_{\odot} \tag{10}$$

roughly the same as the bolometric luminosity of the source, which is  $L_{\rm bol} \sim 3.6 L_{\odot}$  (Froebrich 2005). The jet is likely powered by accretion as in the current jet launching models (see, e.g., Shu et al. 2000; Pudritz et al. 2007), and our result suggests that the jet can indeed carry away a large fraction of the accretion power in the early phase of star formation as pointed

out by Cabrit (2000). Therefore, the accretion rate should be estimated using both the bolometric luminosity of the source and the mechanical luminosity of the jet. Assuming that the source SMM1 is a single protostar with a stellar mass of  $M_* \sim 60~M_{\rm Jup}$  (Froebrich et al. 2003; Paper I) and a stellar radius of  $R_* \sim 2R_{\odot}$  (Stahler 1988; Machida et al. 2008a), then the accretion rate is  $\dot{M}_a \sim (L_{\rm bol} + L_j)R_*/GM_* \sim 8.5 \times 10^{-6}~M_{\odot}~\rm yr^{-1}$ . Thus, the mass-loss rate is estimated to be  $\sim 20\%$  of the accretion rate, consistent with that predicted in the current MHD models (Shu et al. 2000; Pudritz et al. 2007). However, the source SMM1 itself could be a binary (see §4.1). If the jet source has a mass of  $\sim 30~M_{\rm Jup}$  and it is responsible for half of the bolometric luminosity, then the accretion rate toward the jet source is  $\sim 1.3 \times 10^{-5}~M_{\odot}~\rm yr^{-1}$ . In this case, the mass-loss rate is  $\sim 14\%$  of the accretion rate, also consistent with that derived simply from the law of energy conservation and the jet's angular momentum reported in Paper I (e.g., Soker 2009). Further observations are really needed to constrain our estimation.

Now let us check if the accretion rate is acceptable by comparing the accretion time with the outflow dynamical time. If the accretion rate was the same in the past, the accretion time would be  $M_*/\dot{M}_a$ , i.e.,  $\sim 7000$  yrs if the source is single, or  $\sim 2300$  yrs if the source is a binary. The outflow dynamical time can be estimated with the tip of the eastern outflow lobe in H<sub>2</sub> (Hirano et al. 2006) because the bright H<sub>2</sub> emission there requires the shock velocity there to be  $\lesssim 55$  km s<sup>-1</sup>, otherwise H<sub>2</sub> there will be all dissociated (Smith et al. 1991; O'Connell et al. 2005). Therefore, with the tip at  $\sim 12500$  AU from the source, the dynamical time for the outflow is  $\gtrsim 1100$  yrs. As a result, the accretion time is not shorter than the outflow dynamical time, and thus the accretion rate is acceptable. The accretion rate is high probably because of the extremely young age of the source SMM1. Note that, if the source SMM1 is a binary, then in our estimation the accretion time is only two times the outflow dynamical time. If that is the case, the jet could be launched soon after the accretion started.

### 4.3. Origin of SO and SiO emission: shock enhancement

The abundances of SiO and SO in the gas phase are found to be highly enhanced in the jet as compared to the quiescent molecular clouds, even close to within 300 AU from the source where the dynamical time scale is < 10 yrs. Here we discuss the possible origins of the abundance enhancement of these molecules.

Although SiO abundance enhancement has been found in many Class 0 jets, its origin is still not well determined. In HH 211, the abundance enhancement of SiO is closely related to the shocks, with the emission associated with a broad range of velocities. As pointed out

by Schilke et al. (1997) in their early work, the shocks are likely required to generate the SiO gas by either (1) a release of SiO from dust grains, or (2) a release of Si atoms followed by conversion to SiO through gas-phase chemistry. The jet indeed seems to be dusty, with the 352 GHz continuum emission extending along the jet axis from the source (Paper I). Recently, Gusdorf et al. (2008a) have studied the formation time of the SiO from Si via gasphase reactions in stationary C-type shocks with grain sputtering of Si-bearing material for the preshock number density of hydrogen nuclei  $n_{\rm H}=10^4-10^6~{\rm cm}^{-3}$ . From their results, if the shock velocity is greater than 30 km s<sup>-1</sup>, we can approximate the SiO formation time to be roughly given by  $10^7/n_{\rm H}$  yrs. If we extrapolate that SiO formation time for HH 211 that has  $n_{\rm H}=2n\gtrsim 6\times 10^6~{\rm cm}^{-3}$  (see §2.3 for n), then the formation time is  $\lesssim 2~{\rm yrs}$ for HH 211, short enough to produce the SiO emission in the SiO knots. Note that nonstationary C-type shocks (Gusdorf et al. 2008b) and J-type shocks with more sophisticated grain processes (Guillet et al. 2009) could also be responsible for the SiO emission and more studies are needed to explore those possibilities. There is a lack of SiO emission [not only in J=8-7 transition, but also in lower transitions in J=5-4 (Gueth et al. in prep) and J=1-0 (Chandler & Richer 2001)] at the base of the jet in the innermost pair of CO knots, BK0 and RKO. This lack of SiO emission is unlikely due to a lack of material because the jet is expected to have the same density along the jet axis except near the launching point where the density is much higher (Shu et al. 2000). This lack of SiO emission suggests that the SiO is not abundant there in the gas phase. If the SiO were there abundant in the gas phase, the shocks that excite the CO emission (which was also detected in higher transition in the far infrared by Giannini et al. 2001) would also excite the SiO emission.

SO abundance enhancement has also been seen toward other Class 0 sources, e.g., L1448, HH 212, and L1157, because of shocks. In L1157, the SO emission is seen in the prominent bow shocks at  $\gtrsim 20000$  AU away from the source, but no jetlike SO emission is seen around the source (Bachiller et al. 2001). In L1448, the SO emission is seen at shock-precursor and post-shock velocities (Jiménez-Serra et al. 2005). In HH 212, the SO emission at the base is jetlike as in HH 211 and it extends to  $\sim 800$  AU from the source (Lee et al. 2007a). Note that in that source SO emission in lower transition has also been detected upto 8000 AU to the south along the jet (Lee et al. 2006). Thus, the abundance of SO in the jet seems to decrease from the younger sources, e.g., HH 211 and HH 212, to the older sources, e.g., L1157 (which shows no clear jetlike SO emission), like that of SiO (Shang et al. 2007). In L1157, it was proposed that sulfur is released from dust grains in the form of H<sub>2</sub>S in the shocks and that is then oxidized to SO (Bachiller et al. 2001). In L1448, H<sub>2</sub>S emission is present in the shock-precursor, but is missing in the post-shock gas. Jiménez-Serra et al. (2005) considered oxidation of H<sub>2</sub>S to SO in shock, but judged the timescale [100 – 1000 yrs suggested by Wakelam et al. (2004)] too long. They thus proposed that the SO molecules

might be abundant on dust grains and directly released from grains in the shocks. HH 211 and HH 212 could have the same origin of abundance enhancement in SO. In HH 211, the shocks can release sulfur from grains in the form of e.g., H<sub>2</sub>S, and then oxidize it to SO, as proposed in L1157. If the jet is rich in atomic oxygen (OI) and carbon ion (CII) (as can be seen in ISO observations in Giannini et al. 2001), then oxidation of H<sub>2</sub>S to SO could take only a few years. For example, the following sequence would have timescales less than 5 yrs in a shock environment with  $n_{\rm H} \sim 10^6~{\rm cm}^{-3},~T_{\rm gas} \sim 1000~{\rm K},~n({\rm HI})/n({\rm H}_2) \sim 0.01,$  and  $n({\rm OI})/n_{\rm H} \sim 10^{-4}$ : H<sub>2</sub>S + H  $\rightarrow$  HS + H<sub>2</sub>; HS + O  $\rightarrow$  SO + H. In this example, the rate coefficients are  $2.5 \times 10^{-11}$  cm<sup>-3</sup> s<sup>-1</sup> and  $1.3 \times 10^{-10}$  cm<sup>-3</sup> s<sup>-1</sup> (RATE06 by Woodall et al. 2007), and the conversion timescales for  $H_2S \to HS$  and  $HS \to SO$  are 0.13 yrs and 3 yrs, respectively. (The timescale for  $HS + H \rightarrow S + H_2$  is 0.13 yrs, but the timescale for reverse  $S + H_2 \rightarrow HS + H$  is 2.6 yrs at 1000 K. Thus, about 5 percent of sulfur atoms will be in HS in 3 yrs and be available for HS + O.) Again, there is a lack of SO emission at the base of the jet in the innermost pair of CO knots. This suggests that the SO is not abundant there, neither in the gas phase nor on the dust grains. If the SO were there on the dust grains, it would evaporate into the gas phase and then be excited to produce the SO emission.

We now speculate what could cause the lack of SiO and SO abundances in the gas phase at the base of the jet in the innermost pair of CO knots. Since the mass-loss rate in the jet is high ( $\sim 1.8 \times 10^{-6}~M_\odot~{\rm yr}^{-1}$ ), SiO and CO as well could have formed via gas-phase reactions in an initially atomic jet close to the launching point (< 0.1 AU) (Glassgold et al. 1991). If that is the case, the lack of gas-phase SiO in the innermost pair of CO knots suggests that the SiO could be afterward dissociated e.g., by the possible presence of a far-UV radiation field near the source. However, it is also possible that the SiO is rapidly depleted onto the grains or converted to SiO<sub>2</sub> (Gusdorf et al. 2008a) if the temperature of the jet indeed drops rapidly with the distance from the launching point as predicted by Glassgold et al. (1991). In addition, the lack of gas-phase SO in the innermost pair of CO knots also suggests that the SO, if formed at the base, is afterward destroyed. On the other hand, the CO could stay in the gas phase, giving rise to the CO emission even in the innermost pair of CO knots. Both the SiO and SO in the gas phase can form again in the shocks, as discussed above, producing the SiO and SO in the downstream. The SO and SiO abundances in the jet are seen decreasing with the outflow dynamical age, probably because the mass-loss rate decreases with time and so does the formation rate of the SiO and SO molecules.

#### 5. Conclusions

SiO, CO, and SO can all be a good tracer of the HH 211 jet, tracing the internal shocks in the jet. Although the SiO, CO, and SO emissions show roughly the same morphology of the jet, there are detailed differences. In particular, the CO emission traces the jet closer to the source than the SiO and SO emissions. In addition, in the better resolved internal shocks, the CO emission is seen slightly ahead of the SiO emission, likely because the SiO emission traces stronger shocks closer to the shock front and the CO emission traces the weaker shocks in the downstream. In the internal shock where the SO emission is bright, the SO emission appears slightly ahead of the SiO emission, tracing weaker shocks than the SiO emission.

The jet is seen with more than one cycle of wiggle on both sides of the source SMM1 in SiO, CO, and SO. The wiggle is reflection-symmetric about the source and can be reasonably fitted by an orbiting source jet model. The best-fit parameters suggest that the source itself could be a very low-mass protobinary with a total mass of  $\sim 60~M_{\rm Jup}$ . The protobinary may have two equal-mass sources and a binary separation of  $\sim 4.6~{\rm AU}$ , in good agreement with those found in the binaries of very low-mass stars and brown dwarfs.

The abundances of SiO and SO in the gas phase are found to be highly enhanced in the jet as compared to the quiescent molecular clouds, even close to within 300 AU from the source where the dynamical time scale is < 10 yrs. The abundance enhancements of these molecules are closely related to the internal shocks in the jet. The detected SiO is either the consequence of the release of Si-bearing material from dust grains or of its formation via gas chemistry in the shocks. The SO, on the other hand, seems to form via gas chemistry in the shocks.

We thank the SMA staff for their efforts in running and maintaining the array, and the anonymous referee for the precious comments. C.-F. Lee thanks Frank Shu for fruitful conversations and Ngoc Phan-Bao for useful discussion. A.P. is grateful to Joaquín Santiago-García, Robert Estalella and Nuria Huélamo for useful discussions.

#### REFERENCES

Anglada, G., López, R., Estalella, R., Masegosa, J., Riera, A., & Raga, A. C. 2007, AJ, 133, 2799

Bachiller, R., Pérez Gutiérrez, M., Kumar, M. S. N., & Tafalla, M. 2001, A&A, 372, 899

Bouy, H., Martín, E. L., Brandner, W., Zapatero-Osorio, M. R., Béjar, V. J. S., Schirmer, M., Huélamo, N., & Ghez, A. M. 2006, A&A, 451, 177

Cabrit, S. 2000, Ecole d'Aussois 2000: Formation stellaire et physique des étoiles Jeunes.

Chandler, C. J., & Richer, J. S. 2001, ApJ, 555, 139

Close, L. M., Siegler, N., Freed, M., & Biller, B. 2003, ApJ, 587, 407

Fendt, C., & Zinnecker, H. 1998, A&A, 334, 750

Froebrich, D. 2005, ApJS, 156, 169

Froebrich, D., Smith, M. D., Hodapp, K.-W., & Eislöffel, J. 2003, MNRAS, 346, 163

Giannini, T., Nisini, B., & Lorenzetti, D. 2001, ApJ, 555, 40

Glassgold, A. E., Mamon, G. A., & Huggins, P. J. 1991, ApJ, 373, 254

Goodwin, S. P., Kroupa, P., Goodman, A., & Burkert, A. 2007, Protostars and Planets V, 133

Guillet, V., Jones, A. P., & Pineau Des Forêts, G. 2009, A&A, 497, 145

Gusdorf, A., Cabrit, S., Flower, D. R., & Pineau Des Forêts, G. 2008a, A&A, 482, 809

Gusdorf, A., Pineau Des Forêts, G., Cabrit, S., & Flower, D. R. 2008b, A&A, 490, 695

Hirano, N., Liu, S.-Y., Shang, H., Ho, P. T. P., Huang, H.-C., Kuan, Y.-J., McCaughrean, M. J., & Zhang, Q. 2006, ApJ, 636, L141

Ho, P. T. P., Moran, J. M., & Lo, K. Y. 2004, ApJ, 616, L1

Jiménez-Serra, I., Martín-Pintado, J., Rodríguez-Franco, A., & Martín, S. 2005, ApJ, 627, L121

Lee, C.-F., Ho, P. T. P., Beuther, H., Bourke, T. L., Zhang, Q., Hirano, N., & Shang, H. 2006, ApJ, 639, 292

Lee, C.-F., Ho, P. T. P., Hirano, N., Beuther, H., Bourke, T. L., Zhang, Q., & Shang, H. 2007a, ApJ, 659, 499

Lee, C.-F., Ho, P. T. P., Palau, A., Hirano, N., Bourke, T. L., Shang, H., & Zhang, Q. 2007b, ApJ, 670, 1188

Lee, C.-F., Hirano, N., Palau, A., Ho, P. T. P., Bourke, T. L., Zhang, Q., & Shang, H. 2009, ApJ, 699, 1584

Machida, M. N., Inutsuka, S.-i., & Matsumoto, T. 2008a, ApJ, 676, 1088

Machida, M. N., Tomisaka, K., Matsumoto, T., & Inutsuka, S.-i. 2008b, ApJ, 677, 327

Masciadri, E., & Raga, A. C. 2002, ApJ, 568, 733

O'Connell, B., Smith, M. D., Froebrich, D., Davis, C. J., & Eislöffel, J. 2005, A&A, 431, 223

Ohishi, M., & Kaifu, N. 1998, Chemistry and Physics of Molecules and Grains in Space. Faraday Discussions No. 109. The Faraday Division of the Royal Society of Chemistry, London, 1998., p.205, 109, 205

Pudritz, R. E., Ouyed, R., Fendt, C., & Brandenburg, A. 2007, Protostars and Planets V, 277

Raga, A. C., Canto, J., & Biro, S. 1993, MNRAS, 260, 163

Santiago-Garcia, J., Tafalla, M., Johnstone, D., & Bachiller, R. 2009, 495, 169

Schilke, P., Walmsley, C. M., Pineau des Forets, G., & Flower, D. R. 1997, A&A, 321, 293

Schöier, F. L., van der Tak, F. F. S., van Dishoeck, E. F., & Black, J. H. 2005, A&A, 432, 369

Shang, H., Li, Z.-Y., & Hirano, N. 2007, Protostars and Planets V, 261

Shu, F. H., Najita, J., Ostriker, E. C. & Shang, H. 1995, ApJ, 455, L155

Shu, F.H., Najita, J., Shang, H., & Li, Z. -Y. 2000, in Protostars and Planets IV, ed. V. Mannings, A. P. Boss & S. S. Russell (Tucson: University of Arizona Press), 789

Smith, M. D., Brand, P. W. J. L., & Moorhouse, A. 1991, MNRAS, 248, 451

Soker, N. 2009, arXiv:0909.4847

Stahler, S. W. 1988, ApJ, 332, 804

Terquem, C., Eislöffel, J., Papaloizou, J. C. B., & Nelson, R. P. 1999, ApJ, 512, L131

Wakelam, V., Caselli, P., Ceccarelli, C., Herbst, E., & Castets, A. 2004, A&A, 422, 159

Woodall, J., Agúndez, M., Markwick-Kemper, A. J., & Millar, T. J. 2007, A&A, 466, 1197

Ziurys, L. M., Friberg, P., & Irvine, W. M. 1989, ApJ, 343, 201

This preprint was prepared with the AAS LATEX macros v5.2.

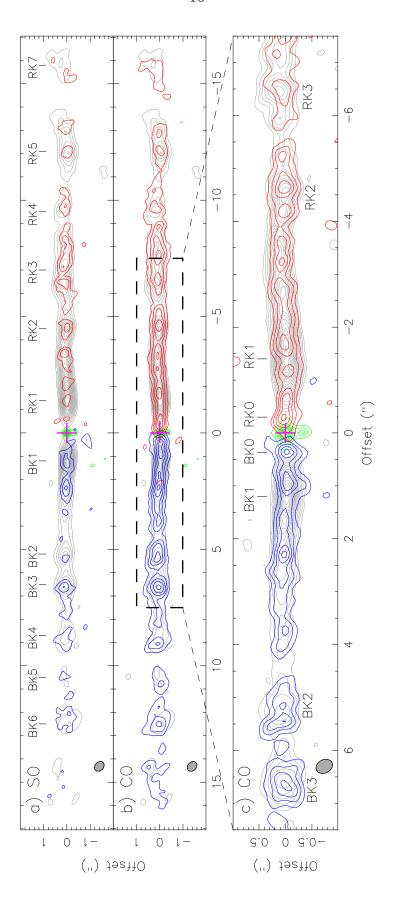


Fig. 1.— SO and CO maps of the jet on top of the SiO map (gray contours) of the jet and the 352 GHz continuum map (green contours) of the envelope-disk from Paper I. The maps have been rotated by 63.4° counterclockwise. The blueshifted and redshifted SiO emission are integrated from -21.2 to 9.2 km s<sup>-1</sup> and from 9.2 to 47.5 km s<sup>-1</sup>, respectively. The cross marks the position of the source SMM1. The knots have the same notations as in Paper I. (a) shows the blueshifted and redshifted SO emission, integrated from -16 to  $9.2 \text{ km s}^{-1}$  and from 14.5 to 43.5 km s<sup>-1</sup>, respectively. No SO emission is detected from 9.2 to 14.5 km/s. The contours start at  $0.52 \text{ Jy beam}^{-1} \text{ km s}^{-1} \text{ with a step of } 0.52 \text{ Jy beam}^{-1} \text{ km s}^{-1}$ . The SiO contours start at 1 Jy beam $^{-1}$  km s $^{-1}$  with a step of 1.5 Jy beam $^{-1}$  km s $^{-1}$ . (b) and (c) show the blueshifted and redshifted CO emission, integrated from -16 to 0 km  $\rm s^{-1}$  and from 20 to 43 km s<sup>-1</sup>, respectively. In (b), the CO contours start at 0.56 Jy beam<sup>-1</sup> km  $s^{-1}$  with a step of 0.84 Jy beam<sup>-1</sup> km  $s^{-1}$ . The SiO contours are the same as in (a). In (c), the CO contours start at  $0.5 \text{ Jy beam}^{-1} \text{ km s}^{-1} \text{ with a step of } 0.5 \text{ Jy beam}^{-1} \text{ km s}^{-1}$ . The SiO contours start at  $0.84 \text{ Jy beam}^{-1} \text{ km s}^{-1} \text{ with a step of } 0.84 \text{ Jy beam}^{-1} \text{ km s}^{-1}$ . The synthesized beams for the lines are  $0.46 \times 0.36$  (natural weighting) in (a) and (b), and  $0.35 \times 0.25$  (super-uniform weighting) in (c).

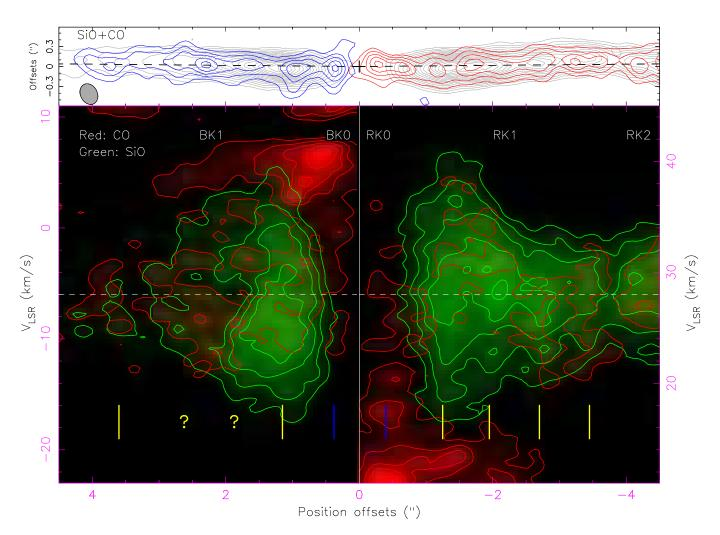


Fig. 2.— PV diagram cut along the jet axis in CO (red image and contours) for the two inner pairs of knots, e.g., BK0, BK1, RK0 and RK1, in comparison to that in SiO (green image and contours). As in Paper I, the yellow lines mark the positions of the sub-knots in knots BK1 and RK1, and the question marks indicate the possible positions of the two sub-knots in knot BK1. The blue lines mark the positions of knots BK0 and RK0. The systemic velocity is 9.2 km s<sup>-1</sup>. The white horizontal dashed lines mark the mean velocities of the jet, which are  $-6 \text{ km s}^{-1}$  on the blueshifted side and  $28 \text{ km s}^{-1}$  on the redshifted side, as given in Paper I. The SiO contours start at 0.15 Jy beam<sup>-1</sup> with a step of 0.15 Jy beam<sup>-1</sup>.

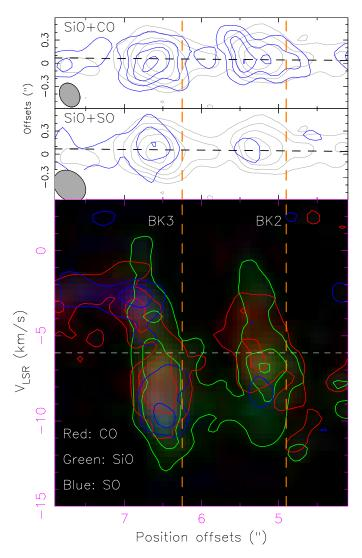


Fig. 3.— PV diagrams cut along the jet axis in CO (red image and contours), SiO (green image and contours), and SO (blue image and contours) for knots BK2 and BK3. The white dashed line indicates the mean velocity for the eastern component of the jet. The orange dashed lines separate the heads and tails for knots BK2 and BK3, as in Paper I. The SiO contours start at 0.15 Jy beam<sup>-1</sup> with a step of 0.15 Jy beam<sup>-1</sup>. The CO contours start at 0.1 Jy beam<sup>-1</sup> with a step of 0.1 Jy beam<sup>-1</sup>. The SO contours start at 0.08 Jy beam<sup>-1</sup> with a step of 0.08 Jy beam<sup>-1</sup>.

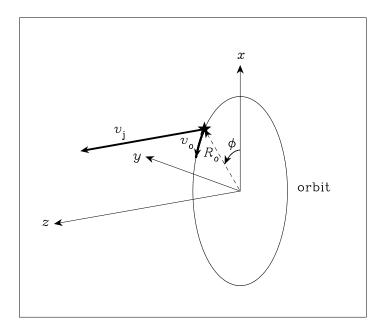


Fig. 4.— Schematic diagram of the orbiting source jet model. Star marks the source position in the orbit.

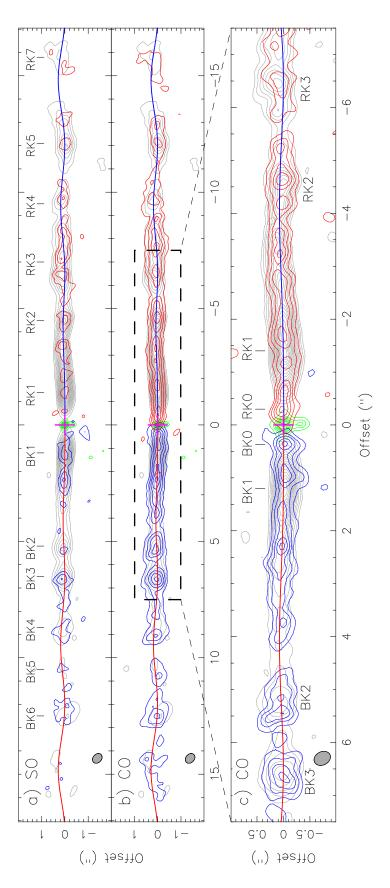


Fig. 5.— The orbiting source jet model for the wiggle plotted on top of Figure 1. The red and blue curves are derived from our best-fit model (see the text in §3).